EMG-Based Intention Detection Using Deep Learning for Shared Control in Upper-Limb Assistive Exoskeletons

Paniz Sedighi, Xingyu Li, and Mahdi Tavakoli,

***Abstract*— In the field of human-robot interaction, surface electromyography (sEMG) provides a valuable tool for measuring active muscular effort. While numerous studies have investigated real-time control of upper extremity exoskeletons based on user intention and task-specific movements, the prediction of body joint positions based on EMG features has remained largely unexplored. In this paper, we address this gap by proposing a novel approach that leverages Convolutional Neural Networks and Long-Short-Term Memory (CNN-LSTM) models to generate exoskeleton joint trajectories. Our methodology involves collecting data from three channels of EMG and three degrees-of-freedom (DoF) joint angles and enables us to position control a pneumatic cable-driven upper-limb exoskeleton, thereby assisting users in various tasks. Through extensive experimentation, our intention-based model demonstrates robust performance across different speeds and is capable of detecting variations in payload and electrode placement. The empirical results yielded from our study underscore the efficacy of our approach, particularly in reducing the EMG levels of the user during different tasks by providing exoskeleton assistance as needed.**

I. Introduction

Robotic exoskeletons have recently gained attention for rehabilitation purposes, assistive robotics, and human power augmentation. The use of upper-limb exoskeletons in industrial environments can prevent injuries and occupational accidents [1]. This improves productivity by providing support and assistance for repetitive or physically demanding tasks. In powered upper-limb exoskeletons, more autonomy and adaptability are needed, especially for physical human-robot interaction (pHRI) [2].

To ensure effective and compliant HRI, we must generate motion trajectories that adapt to the smooth and natural movement patterns of a user [3], [4]. It is challenging to estimate the user's intention during each task, especially with upper-limb exoskeletons. There are multiple strategies for acquiring HRI information and human intention detection. When using motion-based methods [5]–[7] with force/torque sensors, human effort must be separated from gravity torque, friction torque, and inertial torque.

On the other hand, EMG provides a good alternative and can directly measure subtle changes in muscle activity [8]. The advantage of myoelectric control over other methods is that the onset motion intention can be detected earlier than the physical motion of the human. Studies on human intention prediction using EMG signals have mostly concentrated on classification problems [9] such as gesture identification [10] and pattern recognition [11]–[13]. Gestures have limitations accommodating a comprehensive range of motion and do not encompass all potential movements.

Continuous effort mapping, also referred to as proportional myoelectric control offers solutions for situations where the time-varying intentions of the user cannot be adequately addressed by discrete function approximation [14]. Model-based approaches utilizing kinematic [15], [16], dynamic [17], or musculoskeletal [18], [19] models based on human biomechanics have been proposed to decode EMG signals and map them to desired control outputs. Due to the irregular and inhomogeneous shape of the upper extremity, these approaches are limited by high computational costs, repeated calibrations, and susceptibility to external disturbances.

Advancements in machine learning (ML) and deep learning have enabled the extraction of useful features from EMG signals on a user-specific basis, facilitating the decoding of complex movements across multiple DOFs. While many studies use neural networks for myoelectric control, they typically focus on capturing basic statistical features of EMG signals for single-joint control. Such networks often struggle to accurately map inputs for complex multi-DoF exoskeletons. Critically, they lack the ability to adapt in real-time to a user's intention, primarily because they aren't data-driven and can't capture intricate EMG features [20].

Model-free approaches such as convolutional neural networks (CNN) are particularly effective in capturing deep features and correlations among multiple channels of EMG signals [21]. CNN has demonstrated superior efficiency compared to traditional statistical and spectral feature extraction methods [22], [23].

Another popular deep learning method is recurrent neural networks (RNN) which takes the history of the EMG data into account [24], [25]. In some studies, a combination of CNN with long short-term memory (LSTM) is used to model the human-robot interaction [26], [27]. In [28], EMG data was fed to one-dimensional convolutional layers and then passed through two bi-directional LSTM layers to learn the kinematic characteristics of the hand.

While CNN/LSTM approaches have been explored, many lack extensive experimental studies on position tracking, especially considering variations in load and speed. Additionally, continuous effort mapping using EMG for upper-limb movements remains under-researched.

In this work, we provide assistance by predicting exoskeleton joint angles based on the user intention and different features such as load, speed, the initial position of the hand, posture, fatigue, and history of the EMG. We call this "Intention-Based Predictive Assistance", or IBPA. We present a shared control scheme for real-time decoding of EMG signals and generating a trajectory that is the best

representative for the upper extremity. Using a parallel CNN-LSTM architecture, we capture spatial and temporal features of the EMG signals and pass the predicted position to a PD position controller.

This paper is arranged as follows: Section II introduces the framework of IBPA, followed by a detailed discussion of the position controller in Section III. The experimental methodology, designed to evaluate the effectiveness of our proposed method, along with the resulting quantitative analyses and findings, are presented subsequently. We then address the study's implications, limitations, and potential future directions. The article concludes with Section VI.

II. EMG-BASED INTENTION DETECTION

In this section, we explain how we integrate a machine-learning model to predict the movements of the arm using EMG signals based on training on user-specific data. First, we discuss the specifications of the model architecture, and then we explain the training process.

A. Hybrid regression model

Fig. 1 illustrates the schematic of the parallel CNN-LSTM architecture. The model takes three channels of EMG signals and angular position data of each robot joint as inputs. For the 3-DoF system, we have 3 channels for EMG and 3 channels for angular position. Sequential data is segmented into 60 ms windows (30 samples per window) and sliding window steps of 2 ms. As a result, $r_t = 30$ rows represent the sliding window size and $r_s = 6$ columns represent the channels.

A notable feature of EMG signals is the latency between the actual movement and the EMG. The EMG activity is observed before the actual movement occurs [29]. In our application, the time delay was estimated at 150 ms by averaging over 100 random samples of EMG activity followed by movement onset. With a 50 ms delay in the serial communication in the real-time system, we leveraged the 100 ms head-start in addition to 60 ms sequential data for time-series prediction. We predict 450 ms into the future to compensate for the delays associated with the cable friction.

The selection of sequential data for the model is determined through a trial and error process. Longer sequential data may result in higher prediction accuracy, but it also introduces more system delay. This occurs because the model needs to wait for all sequential data to be available before making predictions in real-time implementation. To strike a balance between prediction accuracy and system responsiveness, we buffer 30 time steps with a 2 ms sampling time for our model.

To capture spatial features and correlations among each channel, the CNN block is employed. By using 2-D convolutional layers, but 1-D structured kernels, the extracted features become independent of one another. Hence, the arrangement of sensor data in the segmented input window does not affect the final features and counteracts the effect of cross-talk. The electrode placement matches the most activated biological joints associated with the exoskeleton.

The CNN block consists of two-convolutional layers with a kernel size of 1 × 3 followed by max-pooling layers with a filter size of 1 × 2. Batch normalization and rectified linear unit (ReLU) activation functions are applied after each convolutional layer to introduce non-linearity to the model. Since the CNN captures correlations in signal frequency and amplitude among all inputs, the model is not a simple regression. Instead, it is very robust to arbitrary new movements that it was not trained on.

LSTM is a variant of RNNs, renowned for their efficacy in time series regression tasks due to their ability to propagate temporal information. By leveraging the gated structure and cell state in each LSTM node, they effectively counter the vanishing gradients problem commonly encountered in RNNs. At any given discrete time instance t, the LSTM block takes in sensor data, with each LSTM node's hidden and cell states determined by their previous outputs at $t - 1$.

The LSTM layer, composed of 50 nodes, integrates with a CNN to process the data. Features derived from the CNN are flattened, merged with the LSTM temporal features, and then fed into a fully connected layer with 50 neurons, enabling a holistic integration of CNN and LSTM features in our proposed architecture.

Model hyperparameters were primarily chosen based on engineering considerations and hardware constraints. Kernel sizes in CNN's shallow layers targeted specific signal features, while deeper layers sought broader ones. Although parameters like LSTM hidden units were chosen for simplicity, speed, and accuracy, other settings, such as optimization methods, were informed by existing literature [30].

B. Model Training and Performance Evaluation

The model was trained on the dataset obtained from the experiments in subsection IV-B where the protocols for data gathering are explained. The model was trained for each user separately based on the dataset that was individually collected. After the model is fully trained, angular position and EMG signals are received and passed through the trained model for real-time inference.

Prior to training the model, we perform preprocessing on the EMG dataset to eliminate any noise, artifacts, or bias. We utilized a 2nd-order Butterworth low-pass filter with an 8 Hz cutoff frequency and then normalized the data using the Z-score method.

The target for the regression model is a 1 × 3 matrix, with columns representing the angular position of each robot joint. With the goal of predicting 450 ms into the future, the output of the training data is shifted by 225 samples. The model was trained for approximately 3 hours on a GPU. The learning rate is set to 5e-5, and the model uses the Adams optimizer and a batch size of 25. Learning stops after 51 epochs ($\epsilon < 0.001$). The regression loss is measured using mean squared error (MSE). The CNN, LSTM, and cascaded CNN-LSTM were also tested individually and the hybrid model outperforms both of them with 91.2% accuracy.

The model is trained using approximately 1 million time series data points with a 0.002 seconds sampling time,

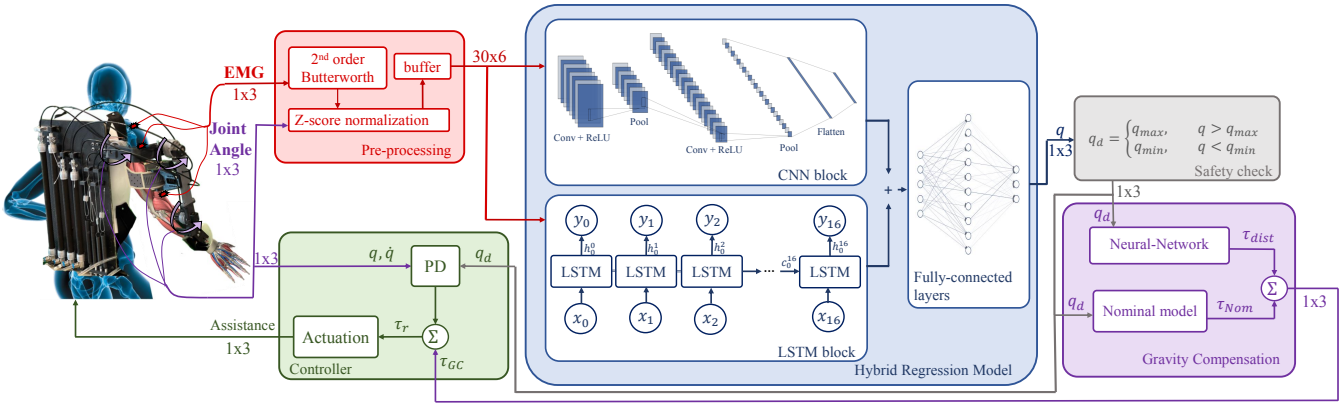

Fig. 1: The schematic of intention-based model control of the upper-limb exoskeleton including the high-level control using hybrid CNN-LSTM and low-level control using Proportional-Derivative (PD) while gravity compensated. During real-time operation, EMG and angular position data are input to the parallel architecture. The predicted angular position is then used to calculate the gravity compensation torque which is used as a feedforward to the position controller. Assistance is provided with pneumatic actuation.

including non-identical movements. The size of the dataset is chosen to include a comprehensive range of human arm movements and incorporate various directions and velocities, thereby ensuring a robust representation of possible motion dynamics. The hyperparameters of the model, such as the number of hidden layers, the optimizer, the learning rate, the parameters related to sequential data, and the number of time steps, are chosen empirically. The system is tested with various future prediction time steps, and 0.45 seconds is determined to be the best response for real-time application.

III. Assistive Robot Control

The objective is to generate a human-like reference path in the configuration space of the human arm and the exoskeleton, specifically focusing on the coordination between the elbow and shoulder. This is achieved by transferring the 7-DoF human joint boundaries into the configuration space of the exoskeleton and the check whether the predicted trajectory fits into the biological joint limits and otherwise using the clipping method (shown in the safety check block in Fig. 1) to ensure the path stays within the specified range.

A. Gravity Compensation

Powering the actuators sufficiently to counteract the joint torque created by the weight of the robot's links is important because when passively collecting the data from the exoskeleton, we discovered that the load of the robot's links and joints on the muscle is affecting the EMG data. Therefore, in order to have unbiased data that isolates EMG from the exoskeleton's load, we implement an AI-modified version of a closed-form gravity compensation model. This means we use a neural network model to capture the difference between the actual dynamics and the nominal model of the robot.

In the presence of gravity and accounting for the dynamics of the human-robot interaction, the equations of motion of the robotic exoskeleton are presented (1) where $M_r \in \mathbb{R}^{N\times N}$ represents the robot's joint inertia matrix, $C_r \in \mathbb{R}^{N\times N}$ denotes the Centrifugal and Coriolis term, and $G_r \in \mathbb{R}^{N\times N}$ is the gravitational term:

$$\mathbf{M}_r(q)\ddot{q} + \mathbf{C}_r(q,\dot{q}) + \mathbf{G}_r(q) = \boldsymbol{\tau}_r - \mathbf{J}^T\mathbf{f}_{int} - \boldsymbol{\tau}_{load} \quad (1)$$

The external force and torque in (1) consists of the actuator torque $\tau_r \in \mathbb{R}^N$ exerted on the exoskeleton's joints, the interaction force f_{int} between the human upper limb and exoskeleton in the Cartesian space, and the torque generated by external load $\tau_{load} \in \mathbb{R}^N$. J is the Jacobian matrix from the end-effector to the joint, and N is the number of DoFs.

Considering there are no inertial and human interactions in the system, the only term left in the equation of motion in a general N-DoF robotic system would be the gravity term. However, due to parameter uncertainty for the closed-form gravity compensation model, there is an error on all joint torques during experiments. To estimate this error, we train a neural network model to predict the torque τ_{dist} needed for the exoskeleton to stay in a certain position. The model is also able to predict the error associated with viscous friction.

By leveraging data acquired from angular encoders, which links to the actuation torque leading to a given configuration, we were able to determine the variation between the data-driven torque and its nominal counterpart τ_{Nom}. Through offline training, this error was then aligned with the angular position data, ensuring that for each robotic configuration, the system recognized both the nominal value and the error as identified by our trained model.

Later during inference and data collection, we use the predicted τ_{dist} with respect to a set of given joint angles q_i to estimate the amount of τ_{GC} needed for gravity compensation.

$$\tau_{GCi} = \tau_{Nomi} + \tau_{dist} \quad (2)$$

B. Trajectory Tracking

A trajectory-tracking controller is designed to follow the predicted position that already overcomes the challenges associated with the pneumatic cable-driven system, including inherent delays, internal friction, and cable elasticity. As shown in Fig. 1, the Proportional-Derivative (PD) control scheme was implemented to follow the predicted joint angles.

In order to provide assistance as needed, the predicted trajectory is followed while compensating for the external load and supporting the exoskeleton's weight. The control law in (3) is designed to follow the predicted trajectory that already takes into account the external load and human effort.

$$\tau_{ri} = K_P(q_{di} - q_i) - K_D\dot{q}_i + \tau_{GCi} \tag{3}$$

The controller employs a PD control scheme with a proportional gain K_P and a derivative gain K_D to follow the desired joint angle q_{di} at every time step. Meanwhile, joint level feedforward gravity compensation τ_{GCi} is utilized to further enhance the control performance by taking advantage of the known system kinematics.

IV. Materials and Experiments

In this section, a 3-DoF soft robotic exoskeleton is used for proof of concept and to evaluate the performance of the user intention-based assistive exoskeleton control approach.

A. Hardware implementation

The hybrid regression network for position prediction and the neural network for gravity compensation is implemented using Python (Python Software Foundation, USA). The neural network predictions are sent to an Arduino Mega 2560. Angular position and EMG signals are captured by the Arduino I/O ports with 50 and 2 kHz respectively. The controller generates assistive gains in real-time with a 500 Hz sampling rate.

The acquired data is transferred to Python via the Pyserial library at a 115200 baud rate, ensuring a communication delay below 10 ms. Multi-threading in Python ensures synchronized data handling, preprocessing, and model predictions. Specifically, the encoder data is down-sampled to align with EMG data. The main thread processes data within a 15 ms window, employing a buffer mechanism to continually update the CNN-LSTM input.

The exoskeleton's joints are powered by fluidic muscles DMSP-20-RM-CM (Festo Corp,Esslingen, Germany. To regulate the pressure of these pneumatic soft actuators, electro-pneumatic transducers EP211-X120-10V (Omega Engineering Inc., USA) are utilized. Quadrature optical encoders (HEDM-5500 B12, Broadcom Inc., US) are attached to the shoulder and elbow joints for measuring the exoskeleton's position. Three SX230-1000 surface EMG sensors (Biometrics Ltd., United Kingdom) are positioned along the medial deltoid, anterior deltoid, and biceps brachii muscles. The sensors are embedded with a built-in 460 Hz low-pass filter.

B. Experimental protocol

Experiments were conducted on one female and one male participant who met specific inclusion criteria, including a lack of musculoskeletal injury or motor-control impairment. The participants were 25 and 22 years of age, 165 cm and 183 in height, and weighed 58 and 91 kg, with an arm length of 55.2 cm and 65.3 cm. The participants provided explicit written informed consent prior to their participation in the study.

Before starting the experiments, the participants' arms were prepared using an alcohol swab to remove surface oils and other contaminants. Subsequently, three EMG electrodes were placed on the medial deltoid, anterior deltoid, and biceps brachii. This muscle combination was chosen based on the highest RMS EMG activation for single joint movements such as lateral raise, frontal raise, and bicep curl in exoskeleton movements [31], [32]. Upon wearing the exoskeleton, EMG and angular position data were collected for two minutes during its static calibration. Throughout the experiment, the exoskeleton consistently remained gravity-compensated using a feedforward loop.

The experiments were structured in two phases: the training phase and the evaluation phase. The former aimed to gather data to train the system on the participants' data and tailor the IBPA to them. The **training phase**, spanning 7 days for each participant, required them to consistently wear the exoskeleton while being seated. Each day comprised multiple sessions with hourly breaks, wherein the participants executed various tasks.

Data collected during training included three channels of EMG and three channels of angular encoders to measure joint positions. Experimental tasks were created using training landmarks shown in Fig. 2. First, a pair of start and end positions were randomly chosen, and the participant was instructed to reach the destination starting from the initial position. Variations in initial position, destination, load, speed, electrode placement, and pause/rest time are termed movement *features*. Each unique combination produced a specific movement, referred to as a training *task*.

In the training phase, only the start and end positions were monitored and the transition (variations in the upper body's angular positions and position of the end effector during movement from the initial point to the destination) was not recorded. In other words, the participant followed an arbitrary desired trajectory that they deemed most convenient. The emphasis was on capturing the user's natural kinematic patterns.

Variations in speed were categorized as slow or fast and were only distinguishable by observation. Upon concluding the training phase, the average speeds of these movements were computed by evaluating the distance traveled relative to the time taken for task completion. Participants tried to maintain consistent speeds across tasks ($v_{slow} = 0.05m/s$, $std = 0.01$ and $v_{fast} = 0.2m/s$, $std = 0.02$). Furthermore, movements were executed both with and without an added 500 g weight across different days, taking into

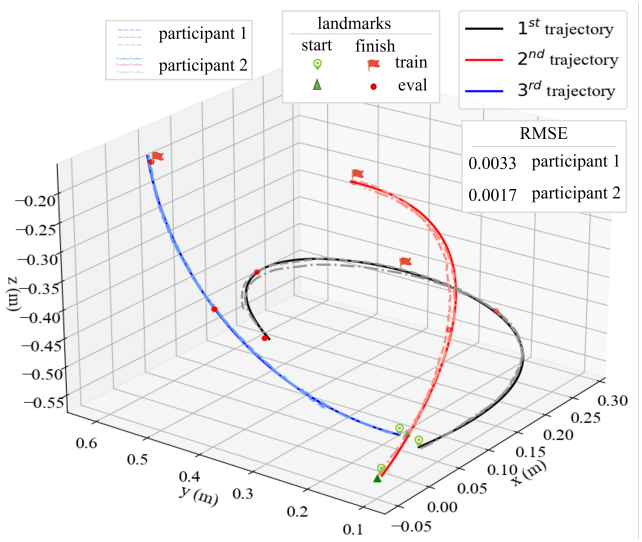

Fig. 2: Landmarks for both experimental phases are shown. Three reference trajectories were defined for the evaluation phase (in bold colors) with specified landmarks for the participants to follow. The dashed and dashed-dotted lines represent the mean trajectories traveled by the first and second participants respectively. Participants followed the reference trajectories with an average root mean square error (RMSE) indicated on the far right table.

account potential variations in EMG electrode placements ($displacement < 10mm$).

The training tasks were designed to activate targeted muscles with different transitions. In total, roughly 600 different tasks were executed, considering all possible variations. Although most of the tasks were completed either with or without a load, during some of the tasks, at a random landmark, the participants were unexpectedly given a load and instructed to place it at a predetermined destination. The participants repeated each at least twice. The collected data for each participant was used to personalize the IBPA further detailed in section II.

The **evaluation phase**, spanning six days within a week, aimed to assess the capability of the deep learning model in facilitating user-initiated movements and providing exoskeleton-based support. Contrary to the training phase, participants encountered three randomly presented conditions: Unassisted (absence of exoskeleton), assisted with exoskeleton gravity compensation (GC), and assisted with IBPA. The same tasks were repeated for all three conditions wherein users had to follow three predefined reference trajectories shown in Fig. 2.

The collected data for the evaluation phase included EMG readings from the same muscles, angular positions, control inputs, and predicted trajectories. Data collection for each trajectory occurred in a single uninterrupted session. It included combined testing tasks that were randomly presented to the participants. The tested *tasks* encompassed varying speeds (0.18 m/s, 0.1 m/s, 0.07 m/s), loads (0.5 Kg, 1 Kg, 1.5 Kg), postures (seated and standing), landmarks, pause/rest time, and electrode placements ($displacement < 10mm$).

During the evaluation phase, the reference trajectories for the end effector (center of the palm) in Cartesian space along with error boundaries ($|e_b| < 15mm$) were shown on a monitor with real-time forward kinematics plots as feedback for the user to maintain their position and speed during movements.

While the tested tasks share some features with the training tasks, we ensured that they also include differences. For instance, the postural difference is not considered during training, or heavier loads are tested during evaluation. To ensure repeatability and the integrity of the experiments, each unique test task was created and repeated five times over the course of three days. Pause, rest, and hold on the landmarks were determined randomly.

V. Results

Experimental results were segmented according to local minimums in joint positions. For each segmented cycle, the root mean square (RMS) value of the EMG, joint angle, and exoskeleton torque were calculated. Recognizing the importance of capturing the variability in performance within individuals, we aggregated the data, averaging the five repetitions of tasks across both male and female participants.

The task was deemed unsuccessful if error bounds around the reference trajectories were exceeded. Successful completion necessitated hitting all landmarks. Across 162 tasks and 810 trials per participant, we observed a 99.9% completion rate.

The statistical significance for the percentage change across exoskeleton conditions was determined using Mixed Model ANOVA with SPSS Statistics 21.0 (IBM, Amonk, NY, USA). Initially, the Shapiro–Wilk test assessed the data's normality, followed by Levene's test to check for homogeneous variances. All the other descriptive information can be found in an appendix on GitHub [1].

The mean and standard deviation of velocities for trajectories 1 to 3 were calculated using the summation of the point-to-point Euclidean distance traveled by the participants divided by the duration of task ($v_1 = 0.181m/s$, $\sigma = 0.013$, $v_2 = 0.099m/s$, $\sigma = 0.006$, $v_3 = 0.069m/s$, $\sigma = 0.005$).

A. Assistive torque comparison

In the context of evaluating the exoskeleton support, we assessed the total torque, which was computed as the summation of joint-specific torques. The hypothesis posits that the exoskeleton actuation torque should be higher for the IBPA method, indicating a greater contribution from the exoskeleton to moving the biological joint.

Our statistical model was structured to only compare the two conditions – IBPA and Gravity Compensated (GC) – given that the No Exo condition inherently lacks associated torque values. The model's fixed effects encompassed the torque responses under the two conditions, with the computed F-statistic for the conditions being $F = 153.976$ ($p < 0.05$).

As shown in Fig. 3, there was a significant increase in torque exertion in most tested tasks for the IBPA compared

[1] https://github.com/tbs-ualberta/RAL-EMG-Based-Intention-Detection.git

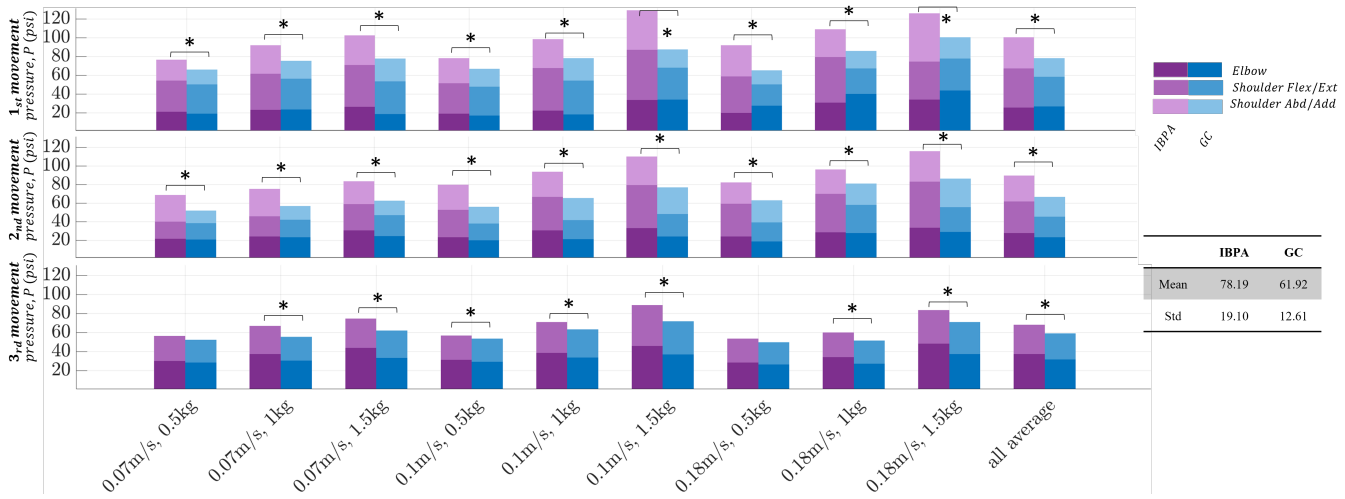

	IBPA	GC
Mean	78.19	61.92
Std	19.10	12.61

Fig. 3: The sum of all joint torques, calculated as the root mean square, was averaged across all repetitions, tasks, and participants for each condition: IBPA-assisted (purple) and GC-assisted (blue). The total torque increase using the proposed IBPA method relative to GC condition is on average 26.2% higher and a significant increase can be seen in almost all variations of tasks. The variations in muscle-specific EMG reduction across all conditions, speed, and load are illustrated through different shades. The average of all tasks is shown on the far right sidebar. The table on the right represents the mean and std across 540 repeated tasks. * represents statistical difference ($p < 0.05$).

with GC. It was evident that the Gravity Compensated (GC) condition recorded a significant torque value of 61.33 psi ($SE = 8.12$, $t = 7.55$, $p = 0.001$). In juxtaposition, the IBPA condition revealed a markedly higher torque of 76.58 psi ($SE = 8.14$, $t = 9.4$, $p = 0.001$).

In a joint-specific analysis, the average assistive torque for shoulder abduction is zero (psi) for the third trajectory, reflecting minimal mid-deltoid activation. For the GC method, torque is distributed as 20%, 40%, and 40% among shoulder abduction, shoulder flexion, and bicep respectively; while for IBPA, the distribution is 22%, 41%, and 35%. Notably, the IBPA predicts a 9% increase in elbow assistance, a 30% rise in actuation across all trajectories for ShFE, and a 47% increment for the initial two trajectories for ShAA.

Delving into the random effects of our model, neither trajectory ($Wald - Z = 0.978$, $p = 0.328$), speed ($Wald - Z = 0.932$, $p = 0.351$), nor weight ($Wald - Z = 0.942$, $p = 0.346$) displayed a significant influence on the total torque, suggesting that the variations in these parameters did not substantially modulate the torque values under the studied conditions.

B. EMG comparison

An additional component of the experiments involves comparing the IBPA method with a no-exoskeleton condition. The performance of the model was examined by variations in speed and load, with comparisons made by measuring EMG during the experiments. EMG levels provide a measure of human effort, and the hypothesis is that they should be lower when using the assistive exoskeleton.

Fig. 4 shows the accumulation of EMG reductions in all muscles across all variations and trajectories between the proposed method and two other conditions.

Statistical analysis shows distinct patterns among the three conditions. The No Exo condition yielded a significant increase in EMG activity ($SE = 0.11$, $t = 12.98$, $p < 0.05$), suggesting a substantial muscular effort in the absence of exoskeleton support. In contrast, the IBPA condition demonstrated a significant reduction in EMG values ($SE = 0.13$, $t = 6.63$, $p < 0.05$), affirming our first hypothesis of attenuated muscular effort when using our proposed method. However, the GC condition did not show a substantial difference from the No Exo condition ($SE = 0.13$, $t = 12.66$, $p < 0.05$),

In transitioning from the GC method to IBPA, average reductions were observed in EMG levels across the three movements: 44.3% for the elbow, 49.8% for ShFE, and 46.9% for ShAA. When comparing the proposed IBPA method with the no exoskeleton condition over three trajectories, there were average reductions of 53.8% for the elbow, 49.6% for ShFE, and 45.1% for ShAA.

Delving deeper into the random effects, we found that while the trajectory and speed did not significantly influence the EMG values, the weight did have a notable impact. Based on the estimates from the covariance parameters, trajectory and speed exhibited no significant effects. Conversely, weight emerged as a significant factor ($WaldZ = 0.783$,$p = 0.001$)

VI. Discussion

With IBPA, user-led control of the upper-limb exoskeleton could be achieved across different testing tasks using wearable EMG and joint angle sensors. An exoskeleton managed by the IBPA consistently reduced user effort and EMG readings compared to conditions without assistance during three different conditions (see Figures 3 and 4).

The results show that the proposed system can effectively interpret user intentions and provide assistance accordingly. Taking into account movement speed and payload, the proposed approach predicts 450 ms ahead of the user's intended position by leveraging the natural latency in EMG

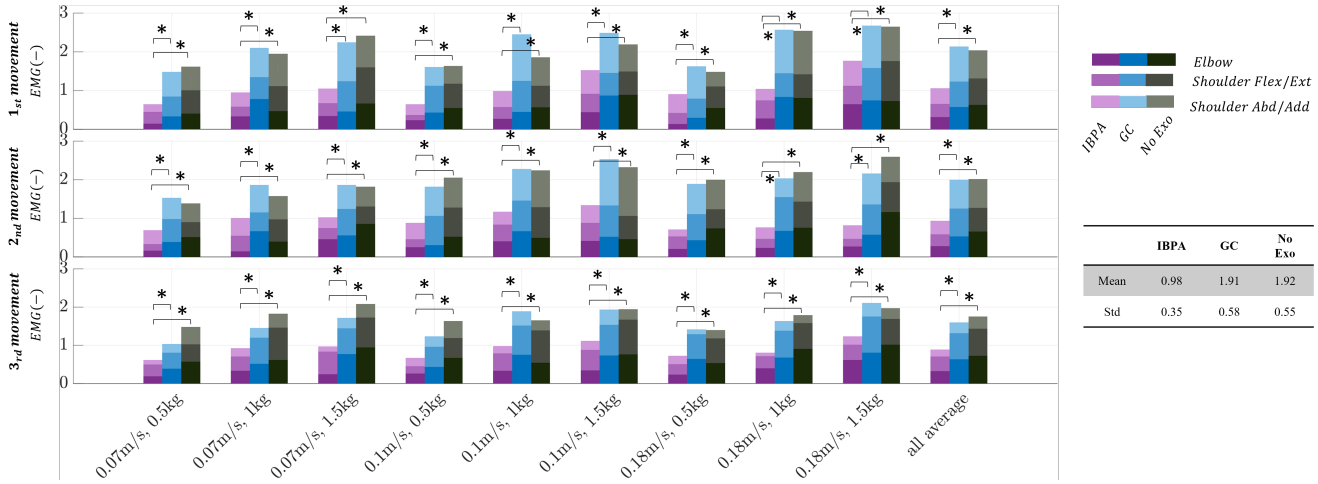

	IBPA	GC	No Exo
Mean	0.98	1.91	1.92
Std	0.35	0.58	0.55

Fig. 4: The reduction in EMG was assessed across all repetitions within each condition, spanning all variations in tasks. The data are indicated for three conditions: assisted by IBPA (in purple), assisted by GC (in blue), and in the absence of the exoskeleton (in black). The results of muscle-specific EMG reduction across all conditions and variations in speed and load are presented in various shades. The table on the right represents the mean and std across 540 repeated tasks. * represents statistical difference ($p < 0.05$)

activity. IBPA allows the exoskeleton's actuation to synergize seamlessly with human muscle contractions, providing a synergistic motion for the biological limb and the exoskeleton. In spite of the complex hysteretic response and nonlinearity arising from the interaction between the cable and the pulley, this approach results in smooth movements.

As shown in Fig. 3, the cumulative joint torque generated by the exoskeleton is generally higher with the IBPA condition. Within each condition, the human and exoskeleton should generate more or less the same amount of joint torque. In the presence of assistance provided by the IBPA method, the user generates lower biological torque. With the implementation of IBPA, the user and exoskeleton consistently reach a state of load sharing. With this cooperation, arm motion is generated more efficiently, reducing both EMG signals and biological torque.

The level of assistive torque for each joint depends on the path and the activated joint(s) within each task. This results in variations in transitions for each trajectory or load. Since the user was putting less effort into their bicep, the elbow experienced the least torque increase in the first trajectory. On the other hand, the opposite can be seen for the second trajectory. With the third trajectory, there is the lowest increase in assistance level by torque, which can be explained by the fact that only two joints are activated.

Using both angular position and EMG signals as input prevents the robot from being biased solely based on EMG activity and sets a ground truth. This is because EMG activity could be similar in different types of situations. For example, while going up or going down, the robot learns to distinguish direction. Since the experiments were performed on different dates, the model was robust to electrode placements and muscle activity profiles that randomly changed every day.

Higher EMG levels can be seen for heavier weights in almost all joints unless the user decides to transfer the weight-lifting effort to other joints. However, no specific trend was observed by increasing the velocity of the arm movement since the inference is fast enough for the model to predict the position within a shorter time frame.

As a result of the proposed assistance, moving at high velocity requires the same effort as moving at low velocity. A faster throughput of manual tasks will not make a user more tired if the total volume of jobs (trials) remains unchanged. In addition, the insignificant difference in EMG levels between the no exoskeleton condition and the GC demonstrates that the gravity compensation method worked.

Fatigue-induced variations in EMG signals could potentially impact the performance of the model. Despite these challenges, our research demonstrated the model's robustness in accommodating such variations. From our experimental findings, the model effectively detects long-term EMG variations including muscle fatigue, and appears to benefit from our approach, which mitigates user fatigue in extended exoskeleton use compared with no exoskeleton conditions. Enhancing the LSTM network with more hidden states captures prolonged temporal shifts, and future research will delve deeper into fatigue effects. Additionally, to ensure voluntary control of the exoskeleton torque, the user could indicate the desired support ratio as a trade-off between comfort and assistance.

In the experiments, the system was trained on two modes of speed and tested on three modes, demonstrating its ability to detect speed. Furthermore, the model was trained with a 500 g load and tested with 0.5 kg, 1 kg, and 1.5 kg. Aside from hardware limitation (maximum actuation: 120 psi with maximum torque of 40 N), lower performance was recorded with loads heavier than 3 kg. The main reason for this is insufficient data. This could be addressed by collecting more data that incorporates variations with heavier loads. Advanced techniques encompass the integration of attention mechanisms or domain adaptation for enhanced generalization.

Based on the experimental results, it was seen that EMG activity of each individual can be decoded and shared control can be achieved with high accuracy for both participants. However, the model has to be trained for each user separately. In other words, the model's performance may not be optimized when utilized by an individual other than the one whose electromyographic profiles were trained on. This is attributed to the distinct EMG thresholds and muscle characteristics inherent to each individual. In the future, methodologies such as transfer learning and domain adaptation will be leveraged to efficiently personalize the model to new EMG thresholds using less data.

Our model's architecture can be designed for modularity, enabling the inclusion of additional EMG channels or more degrees of freedom. While this offers scalability, it also necessitates corresponding enhancements in the training dataset and potentially requires optimized computational solutions. We plan to investigate this scalability in subsequent studies, ensuring model robustness with expanded input dimensions.

Future research will also delve deeper into hyperparameter exploration, ablation studies, and model performance in terms of EMG activity and torque enhancement. While this paper didn't focus on exhaustive machine learning evaluation, we compared three architectures.

VII. Conclusion

Research presented here demonstrated the development of an Intention-Based Predictive Assistance (IBPA) to prevent worker injury while using upper-limb exoskeletons in shared control tasks. The study, which encompassed the utilization of a deep learning model for high-level control and a PD controller with gravity compensation for low-level control, demonstrated promising results in the prediction of user intention and assistance of load-bearing tasks in a variety of situations. The study confirmed the two hypotheses in the experiments. First, significant EMG reductions were obtained across different speed modes and payloads when the proposed exoskeleton assistance method was used. Second, an increase in the exoskeleton torque within all tasks was achieved. Results showed the proposed method's ability to dynamically adapt to the mechanical and biological demands of each task over unseen tasks as required in real-world industrial environments.

References

[1] S. Spada *et al.*, "Investigation into the applicability of a passive upper-limb exoskeleton in automotive industry," *Procedia Manufacturing*, vol. 11, pp. 1255–1262, 2017.

[2] C. Mokri *et al.*, "Muscle force estimation from lower limb emg signals using novel optimised machine learning techniques," *Medical & biological engineering & computing*, vol. 60, pp. 683–699, 2022.

[3] F. Nazari *et al.*, "Applied exoskeleton technology: A comprehensive review of physical and cognitive human-robot interaction," *IEEE Transactions on Cognitive and Developmental Systems*, pp. 1–1, 2023.

[4] W. Wendong *et al.*, "Design and verification of a human–robot interaction system for upper limb exoskeleton rehabilitation," *Medical Engineering & Physics*, vol. 79, pp. 19–25, 2020.

[5] Y. Wang *et al.*, "Extracting human-exoskeleton interaction torque for cable-driven upper-limb exoskeleton equipped with torque sensors," *IEEE/ASME Transactions on Mechatronics*, vol. 27, no. 6, pp. 4269–4280, 2022.

[6] M. Sharifi *et al.*, "Adaptive cpg-based gait planning with learning-based torque estimation and control for exoskeletons," *IEEE Robotics and Automation Letters*, vol. 6, no. 4, pp. 8261–8268, 2021.

[7] J. K. Mehr *et al.*, "Intelligent locomotion planning with enhanced postural stability for lower-limb exoskeletons," *IEEE Robotics and Automation Letters*, vol. 6, no. 4, pp. 7588–7595, 2021.

[8] K. Gui *et al.*, "A practical and adaptive method to achieve emg-based torque estimation for a robotic exoskeleton," *IEEE/ASME Transactions on Mechatronics*, vol. 24, no. 2, pp. 483–494, 2019.

[9] A. Asghar *et al.*, "Review on electromyography based intention for upper limb control using pattern recognition for human-machine interaction," *Proceedings of the Institution of Mechanical Engineers, Part H: Journal of Engineering in Medicine*, vol. 236, no. 5, pp. 628–645, 2022.

[10] B. Chen *et al.*, "Volitional control of upper-limb exoskeleton empowered by EMG sensors and machine learning computing," *Array*, vol. 17, p. 100277, 2023.

[11] E. Rahimian *et al.*, "Hand gesture recognition using temporal convolutions and attention mechanism," in *ICASSP 2022*, 2022, pp. 1196–1200.

[12] Z. Li *et al.*, "Intelligent Classification of Multi-gesture EMG Signals Based on LSTM," *2020 AIEA*, vol. 00, pp. 62–65, 2020.

[13] S. Zabihi *et al.*, "Light-weighted CNN-Attention based architecture for Hand Gesture Recognition via ElectroMyography," *arXiv*, 2022.

[14] J. Fu *et al.*, "Myoelectric Control Systems for Upper Limb Wearable Robotic Exoskeletons and Exosuits—A Systematic Review," *Sensors (Basel, Switzerland)*, vol. 22, no. 21, p. 8134, 2022.

[15] R. S. Zarrin *et al.*, "Towards autonomous ergonomic upper-limb exoskeletons: A computational approach for planning a human-like path," *Robotics and Autonomous Systems*, vol. 145, p. 103843, 2021.

[16] J. Liu *et al.*, "EMG-Based Continuous and Simultaneous Estimation of Arm Kinematics in Able-Bodied Individuals and Stroke Survivors," *Frontiers in Neuroscience*, vol. 11, p. 480, 2017.

[17] S. Qiu, "Exoskeleton Active Walking Assistance Control Framework Based on Frequency Adaptive Dynamics Movement Primitives," *Frontiers in Neurorobotics*, vol. 15, p. 672582, 2021.

[18] L. Wang *et al.*, "Prediction of joint moments using a neural network model of muscle activations from emg signals," *IEEE Transactions on Neural Systems and Rehabilitation Engineering*, vol. 10, no. 1, pp. 30–37, 2002.

[19] G. Durandau *et al.*, "Neuromechanical Model-Based Adaptive Control of Bilateral Ankle Exoskeletons: Biological Joint Torque and Electromyogram Reduction Across Walking Conditions," *IEEE Transactions on Robotics*, vol. 38, no. 3, pp. 1380–1394, 2022.

[20] Z. Tang *et al.*, "An Upper-Limb Power-Assist Exoskeleton Using Proportional Myoelectric Control," *Sensors*, vol. 14, no. 4, pp. 6677–6694, 2014.

[21] A. Ameri *et al.*, "Regression convolutional neural network for improved simultaneous EMG control," *Journal of Neural Engineering*, vol. 16, no. 3, p. 036015, 2019.

[22] Z. Lei, "An upper limb movement estimation from electromyography by using BP neural network," *Biomedical Signal Processing and Control*, vol. 49, pp. 434–439, 2019.

[23] J. Liu *et al.*, "EMG-Based Real-Time Linear-Nonlinear Cascade Regression Decoding of Shoulder, Elbow, and Wrist Movements in Able-Bodied Persons and Stroke Survivors," *IEEE Transactions on Biomedical Engineering*, vol. 67, no. 5, pp. 1272–1281, 2019.

[24] Y.-X. Liu *et al.*, "Muscle synergies enable accurate joint moment prediction using few electromyography sensors*," *2021 IROS*, vol. 00, pp. 5090–5097, 2021.

[25] L. Jia *et al.*, "Individualized Gait Trajectory Prediction Based on Fusion LSTM Networks for Robotic Rehabilitation Training," *2021 AIM*, vol. 00, pp. 988–993, 2021.

[26] M. SimÃo *et al.*, "EMG-based online classification of gestures with recurrent neural networks," *Pattern Recognition Letters*, vol. 128, pp. 45–51, 2019.

[27] A. Nasr *et al.*, "MuscleNET: mapping electromyography to kinematic and dynamic biomechanical variables by machine learning," *bioRxiv*, p. 2021.07.07.451532, 2021.

[28] N. K. Karnam *et al.*, "EMGHandNet: A hybrid CNN and Bi-LSTM architecture for hand activity classification using surface EMG signals," *Biocybernetics and Biomedical Engineering*, vol. 42, no. 1, pp. 325–340, 2022.

[29] D. Farina *et al.*, "The extraction of neural strategies from the surface

EMG," *Journal of Applied Physiology*, vol. 96, no. 4, pp. 1486–1495, 2004.

[30] A. Zhang *et al.*, "Upper Limb Movement Decoding Scheme Based on Surface Electromyography Using Attention-Based Kalman Filter Scheme," *IEEE Transactions on Neural Systems and Rehabilitation Engineering*, vol. 31, pp. 1878–1887, 2023.

[31] G. Coratella *et al.*, "Biceps brachii and brachioradialis excitation in biceps curl exercise: Different handgrips, different synergy," *Sports (Basel, Switzerland)*, vol. 11, no. 3, p. 64, 2023.

[32] G. Coratella, "An electromyographic analysis of lateral raise variations and frontal raise in competitive bodybuilders," *International journal of environmental research and public health*, vol. 17, no. 17, p. 6015, 2020.